Vacuum ultraviolet photoionization and ab initio Investigations of methyl tert-butyl ether (MTBE) clusters and MTBE–water clusters

ARTICLE *in* CHEMICAL PHYSICS LETTERS · MARCH 2013

Impact Factor: 1.9 · DOI: 10.1016/j.cplett.2013.01.025

2 AUTHORS, INCLUDING:

Attila Bende
National Institute for Research and Develo…

66 PUBLICATIONS **368** CITATIONS

SEE PROFILE

Chemical Physics Letters 561–562 (2013) 18–23

Contents lists available at SciVerse ScienceDirect

Chemical Physics Letters

journal homepage: www.elsevier.com/locate/cplett

Vacuum ultraviolet photoionization and *ab initio* Investigations of methyl tert-butyl ether (MTBE) clusters and MTBE–water clusters

Tonia M. Di Palma [a,*], Attila Bende [b]

[a] Istituto Motori, CNR, Via Marconi 8, 80125 Napoli, Italy
[b] Molecular and Biomolecular Physics Department, National Institute for R&D of Isotopic and Molecular Technologies, Donath Street, No. 65-103, RO-400293 Cluj-Napoca, Romania

ARTICLE INFO

Article history:
Received 19 November 2012
In final form 15 January 2013
Available online 25 January 2013

ABSTRACT

The structures and energetics of neutral, ionized and protonated methyl tert-butyl ether (MTBE) clusters and $(MTBE)_m(H_2O)_n$ clusters are investigated by tunable vacuum-UV photoionization mass spectrometry and DFT calculations. While the mass spectra of bare MTBE clusters show unprotonated and protonated clusters ions, the mass spectra of mixed clusters show protonated ions that exhibit magic numbers that correspond to $n = m - 2$ combinations. *Ab initio* calculations show that in the larger clusters a multiple proton transfer leads to a protonated water core where all available hydrogen bonds interact with MTBE molecules. The resulting bond structure explains the cluster stability.

1. Introduction

Methyl tert-butyl ether (MTBE) is an important industrial compound that has been used mainly as a gasoline additive, ever since the 1970s in place of the lead compounds, in order to increase the combustion efficiency and to reduce the toxicity of the exhaust [1]. However, the massive use of MTBE, combined with its high water solubility (4.8×10^4 mg/L), its high vapor pressure near room temperature (0.2 atm at 20 °C) and its low biodegradability, has caused considerable pollution in surface water, rainwater, in snow [2] and also, at significant amounts, in the troposphere [3]. The growing concern over the public health dangers related to the water contamination have inspired many experiments on the possible carcinogenic effects of MTBE [1,4,5] as well as investigations on the degradation of MTBE in water [6].

Few studies on the interactions inside the MTBE–water clusters have been reported [7]; such studies aim at elucidating basic issues such as the MTBE solvation by water or the incidence of this polar compound as a possible seed for water condensation in the atmosphere.

Mass spectrometry coupled with threshold photoionization provides valuable spectroscopic information that, combined with DFT calculations, helps to elucidate structures, stability, physical and chemical properties of molecules and clusters [8]. Dimethyl ether and diethyl ether–water clusters have also been studied in the past [9–11]. In these studies, the formation of stable ion clusters has been interpreted in terms of a proton transfer reaction inside the ionized cluster that leads to the formation of protonated water core ions [11]. MTBE, other than being a widespread pollutant, is also an interesting chemical compound having two different alkyl groups with different hydrophobicity properties. Different reactivities and potentially a more complex proton transfer reaction inside of the ionized clusters are expected.

Here, we present the results of mass spectrometry combined with tunable VUV photoionization on MTBE–water clusters. *Ab initio* calculations are also performed to understand the structure and the stability of the detected clusters. In addition, the DFT study has shown a picture of the ionization involving a proton transfer between MTBE molecules and from MTBE to water.

2. Experimental set-up

The experimental details have been extensively reported in previous works [12–14]. Briefly, the experiments have been carried out by means of time of flight (TOF) mass spectrometry combined with incoherent tunable VUV ionization of a molecular beam.

The mass spectrometer is a linear Wiley McLaren TOF equipped with time-lag focusing and Einsel lenses having an overall mass resolution $\Delta m/m$ (at m/z 128) ≈400.

Pure MTBE or mixed water–MTBE clusters have been produced in the supersonic expansion of vapor mixed using a carrier gas by bubbling He at 4 bar and at room temperature in a reservoir containing pure MTBE (Sigma Aldrich, anhydrous 99.9%) or in a couple of reservoirs containing distilled water and MTBE, separately. A 0.4 mm dia. skimmer has been used to select a molecular beam collinearly with the TOF axis. The clusters in the molecular beam are then ionized by tunable VUV radiation [15].

The VUV radiation is emitted by a plasma produced by focusing a Nd-YAG laser (1064 nm, 10 ns, 300 mJ) on a pulsed supersonic xenon jet (Parker mod. 99, Δt = 400 μs aperture, 10 bar stagnation

* Corresponding author. Fax: +39 0812396097.
E-mail addresses: t.dipalma@im.cnr.it, tonia.dipalma@gmail.com (T.M. Di Palma).

0009-2614/$ - see front matter © 2013 Elsevier B.V. All rights reserved.
http://dx.doi.org/10.1016/j.cplett.2013.01.025

pressure). The emitted radiation is collected by a flat field grating (Horiba, 600 groove/mm, 70 mm diameter) and dispersed in the interaction region as detailed described in [12,13]. The spectral resolution is ±3 nm at 120 nm (±0.2 eV at 9 eV) on the first order of the grating, and ±1.5 nm (±0.1 eV) on the second order at the same wavelength. A DAQ card (National Instruments PCI 5152) was used for data acquisition. The mass spectra were accumulated on 1000 laser shots as functions of the ionizing photon wavelength. For each detected mass peak, the photoionization efficiency (PIE) curve was obtained by reporting the peak area as a function of the ionizing energy. The PIE measurements were performed at a higher resolution on the grating's second order for the most intense signals, otherwise on the first order. The ionization energy (IE) of the MTBE monomer and dimer and the onsets of the fragments appearance in the mass spectrum were obtained from the PIE curve onsets of the respective ions. The PIE curve onsets were here retrieved at the condition S/N≈1, namely when the overall signal (S + N) doubles the background baseline (N) at low photon energy.

3. Computational details

The geometry optimization of the neutral and ionized methyl-tert-butyl-ether (MTBE) molecular oligomers and their water complexes was performed using the M06-2X [16] exchange–correlation DFT functional with the def2-TZVP [17] basis set. The ionization potentials, intermolecular interaction energies and geometry parameters were obtained with the def2-TZVPD [18] basis set. The M06-2X DFT functional calculations were performed using the NWChem [19] molecular modeling program package; software specific basis sets were obtained from the EMSL basis set database [20]. The charge distribution analysis was performed by natural population analysis (NPA) [21,22] using the NBO module [23] built in the NWChem package. Bond dissociation energies (BDEs) were calculated based on the enthalpy difference between the bound molecular system and the dissociated components. Zero-point vibrational energy corrections were applied. Molecular structures were visualized and analyzed using the open source Gabedit [24] molecular graphics program.

4. Results

4.1. Experimental results

As is observed during the ionization of hydrogen-bonded clusters [25,26], the proton transfer in MTBE and MTBE–water clusters is the dominant reaction after photoionization. The predominance of this reaction leads to dissociation of the ionized clusters and the detection of fragments, which are mainly protonated masses. Kinetic effects may also alter the shape of the mass peak, which, in turn, may not allow the unambiguous detection of unprotonated masses, if any. In addition the activation barrier of photodissociation leads to overestimated values of the fragment appearance energy (AE) of a given amount of energy, which is known as 'kinetic shift' [27]. On the other hand, internal energy effects contribute to red-shifted AE values. Then, the AE values of fragments are related to the measured PIE curve onsets of fragments, but in a not trivial manner which can be correctly evaluated only in different and more appropriate experiments [28]. Here, the PIE curve onsets are retrieved as previously described and indicate the photon energy at which, in our experimental conditions, the peaks of the fragments arise in the mass spectra.

In Figure 1a, the mass spectrum of MTBE expanded in a supersonic beam at 10.6 eV photon energy is reported. The main peaks detected in the spectrum that were accumulated after 3000 laser shots are at m/z = 73, 88, 119, and 176. The peaks correspond to the fragment from the parent molecule losing a methyl group from

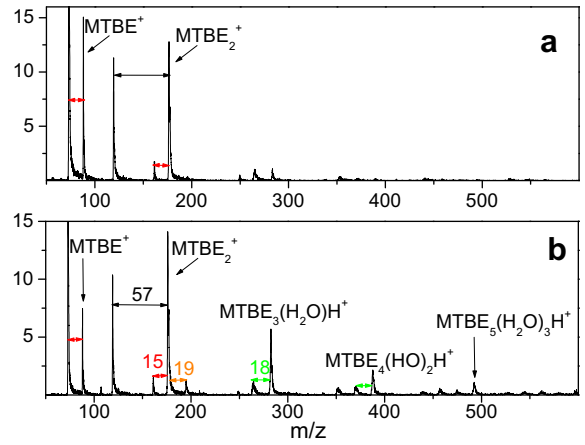

Figure 1. Mass spectrum of pure MTBE vapor (a) and MTBE–water vapor (b) expanded in a supersonic beam. The ionizing photon energy was 10.6 eV. Horizontal arrow colors indicate the mass difference between peaks. Red indicates Δm = 15 u. Black arrows indicate Δm = 57 u. Green arrows indicate Δm = 18 u. Orange arrows indicate Δm = 19 u. (For interpretation of the references to color in this figure legend, the reader is referred to the web version of this article.)

a *t*-butyl group [29] (m/z = 73), to the parent molecule (m/z = 88) and to the non-protonated dimer (m/z = 176). On the tail of the dimer signal, a small peak at m/z 177 is detected, which corresponds to the protonated dimer. The peak at m/z = 119 is most likely a fragment of a heavier cluster that had lost a *t*-butyl radical. Weaker peaks for M_n^+ or M_nH^+ (M = MTBE) are also observed. With the exception of the peaks at m/z = 88, 119 and 176, all the peaks are quite broad; therefore, in our experimental conditions, it is difficult to assign them to clusters or their protonated versions. However, we expect that the photoionization of neutral MTBE clusters creates mainly unstable M_m^+ cations, similar to those produced during the ionization of different ether clusters [9,10]. These clusters undergo intracluster charge redistributions that result in the formation of protonated fragments i.e., $M_{m-n}H^+$. We noted a pattern of cluster fragmentation qualitatively similar to the pattern of fragmentation of MTBE with very low abundance. In fact, peaks corresponding to $(M_n–CH_3)^+$ are detected. In addition, trace amounts of water in the sample were responsible for the observation of a monohydrate cluster $M_3(H_2O)H^+$ at m/z 283 and the small satellite peaks near the tetramer and pentamer.

In Figure 1b, the mass spectrum, at the same photon energy as in Figure 1a, of MTBE vapor mixed with water vapor at room temperature and expanded in a supersonic beam is reported. In addition to the peak observed by expanding the net MTBE vapor, the main cluster series consisted of $M_m(H_2O)_nH^+$ ($n = m - 2$). Other small peaks, separated by 18 mass units and grouped at the left side of the main $M_m(H_2O)_nH^+$ peaks, were recorded. The cluster distribution corresponds to stable structures of cluster ions with the combination of $n = m - 2$ for $M_m(H_2O)_nH^+$, as found by Stace and Moore [9] in the case of different ether–water clusters and as we verified with *ab initio* calculations.

In Figure 2, the PIE spectra acquired by using the second-order grating radiation are reported for the most intense peaks detected in the mass spectra of the supersonic expansion of MTBE/water vapors at room temperature. We remark that no significant differences are observed in the PIE spectra of homogeneous MTBE clusters detected by expanding MTBE/water vapors or net MTBE vapors. We note that, even if the main mixed MTBE–water cluster mass distribution is not affected as a whole, the ion signals are strongly dependent on the expansion conditions. Such conditions include the stagnation pressure and the room temperature, which affect both the MTBE concentration and the cooling of the supersonic expansion. As a result, some PIE shapes may be affected. In

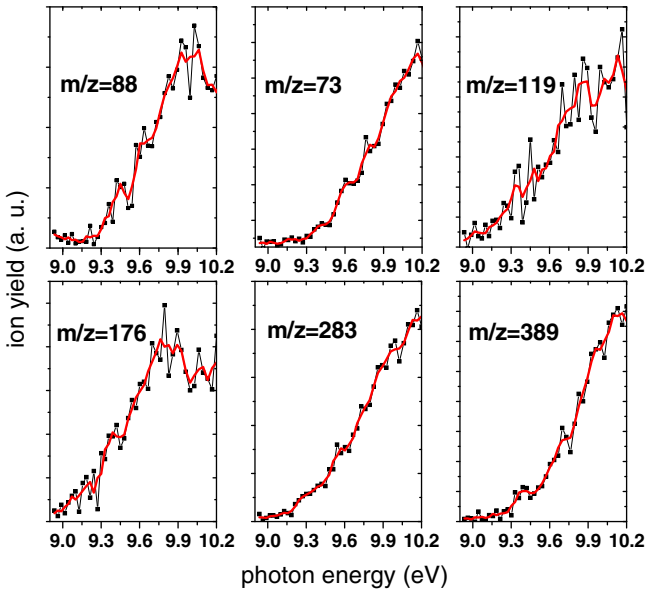

Figure 2. PIE spectra of the most intense clusters detected in the expansion MTBE/water mixture. Straight red lines are the three point adjacent averaging smoothings. (For interpretation of the references to color in this figure legend, the reader is referred to the web version of this article.)

our experimental conditions, namely 4 bar He stagnation pressure and 20 °C room temperature, we observe the parent ion in all of the investigated ionizing wavelength ranges (approximately 1 eV above ionization threshold). However, while the PIE shape of the main MTBE fragment at m/z 73 reproduces the results reported in literature regarding the photoionization cross section of MTBE [30], the PIE shape of the MTBE monomer is different from the results in Ref. [29] on the photoionization of deuterated MTBE. This difference may be due overall to smoothing effects of our lower energy resolution on the PIE shape and to the different cooling of the supersonic expansion.

The photoionization efficiency measurements have been performed by using the VUV radiation diffracted by the second order of the grating (ΔE = ±0.1 eV) for the most intense peaks detected in the mass spectra and on the first order of the grating (ΔE = ±0.2 eV) for the less intense peaks. A list of the assigned peaks and some of the measured PIE curve onsets have been reported in Table 1. From these results, the PIE onset of the detected cluster peaks are comparable or lower than the measured ionization energy of the MTBE monomer with the exception of the peak at m/z = 107 and m/z = 161, which have PIE curve onsets at 9.5 ± 0.2 and 9.4 ± 0.2 eV, respectively.

Table 1
Assigned mass peaks and PIE curve onsets.

m/z	Assigned peaks	PIE curve onset (eV)
73	$(M–CH_3)^+$	9.3 ± 0.1
88	M^+	9.3 ± 0.1
107	$M(H_2O)H^+$	9.5 ± 0.2
119	$M_2–C(CH_3)_3^+$	9.2 ± 0.1
161	$M_2–CH_3$	9.4 ± 0.2
176	M_2^+	9.1 ± 0.1
195	$M_2(H_2O)H^+$	9.6 ± 0.2
249	$M_3–CH_3^+$	
263–266	M_3H^+	9.3 ± 0.2
283	$M_3(H_2O)H^+$	9.2 ± 0.1
352–354	M_4H^+	
370–373	$M_4(H_2O)H^+$	
388–390	$M_4(H_2O)_2H^+$	9.3 ± 0.1
438–444	M_5H^+	
457–462	$M_5(H_2O)H^+$	
475–479	$M_5(H_2O)_2H^+$	
493–496	$M_5(H_2O)_3H^+$	9.2 ± 0.2

4.2. Computational results

4.2.1. MTBE monomer and dimer

For the MTBE monomer, we have computed the equilibrium geometry of the neutral and ionized structures. The geometry of the neutral MTBE and its atomic indices are presented in Figure 3a, while the ionized case is shown in Figure 3b. First, we have calculated the vertical and adiabatic ionization potentials (IPs) of the MTBE monomer. The values are 9.60 eV for the vertical IE and 9.30 eV for the adiabatic IP. Comparing the charge distribution for the ionized MTBE in the neutral geometry configuration and the ionized MTBE in its optimized geometry, one can observe significant charge rearrangement. Immediately after the MTBE ionization, the absence of the electron will be mostly localized on the oxygen atom (0.50e), as well as on one of the protons from the methoxy group (0.1e). After the geometry relaxation takes place, the electron deficiency is redistributed, the electron absences on the oxygen atom is 0.37e and on the C_5 Carbon atom is 0.14e, while on the other atoms, this absence is less than 0.1e. This charge redistribution also leads to significant changes in the bond distances: the C_1–O bond lengthens with 0.016 Å, the C_2–O bond compresses with 0.058 Å, while the C_5–C_2 bond lengthens with 0.116 Å. The BDE study of the MTBE monomer shows that the C_5–C_2 bond can dissociate much easily than the C_2–O bond: E^{BDE}_{C-C} = 0.45 eV, while E^{BDE}_{C-O} = 3.4 eV.

As a next step, we performed similar investigations on the MTBE dimer complex as was performed for the monomer. The equilibrium geometry of the neutral and ionized dimer structures are shown in Figure 3c and d. For the ionized complex, the neutral configuration was chosen as the starting geometry. During the optimization, we observed a proton transfer from one MTBE monomer to the other (see Figure 3d) obtaining a complex built by a protonated MTBE and $(CH_3)_3$–C–O–CH_2. Here, the first molecule (the protonated MTBE) will be positively charged (0.86e) with a complete close shell electron configuration, while the second molecule is almost neutral and has only 0.14e on it but is incomplete at the double occupied electron level. The intermolecular interaction energy between the two molecular systems is −23.84 kcal/mol, which is given by the strong electrostatic interaction between

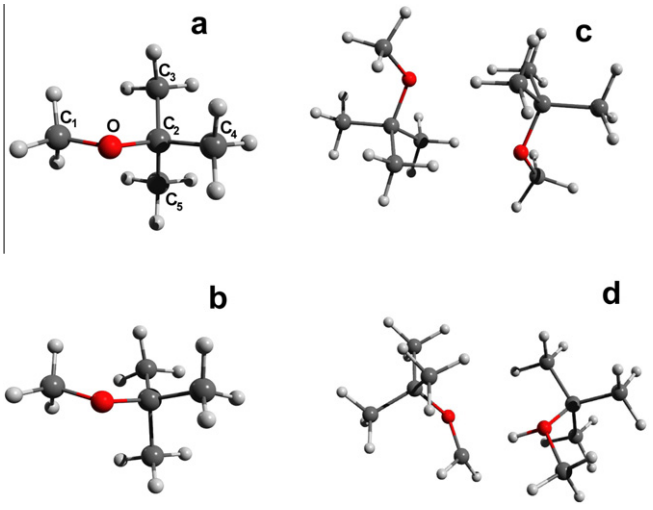

Figure 3. The equilibrium geometric structures of the neutral (a) and ionized (b) MTBE molecule and of the neutral (c) and ionized (d) MTBE dimer.

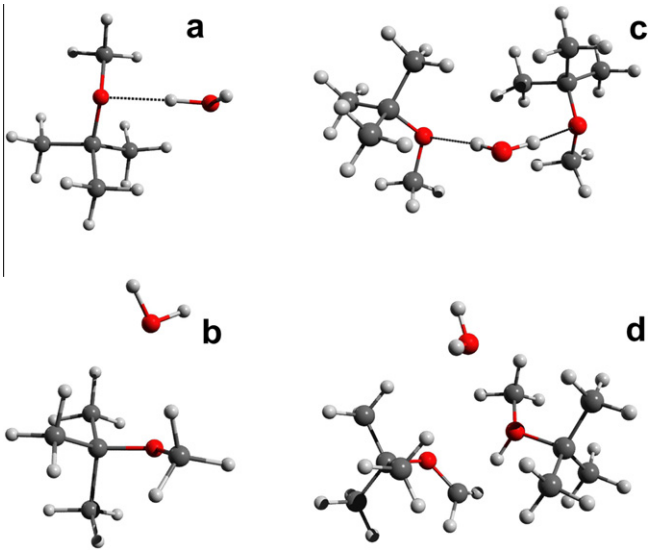

Figure 4. The equilibrium geometric structures of the neutral (a) and ionized (b) MTBE–water complex and of the neutral (c) and ionized (d) MTBE–water clusters.

MTBE–H^+ and $(CH_3)_3$–C–O–CH_2. The vertical IP for the MTBE dimer is 9.25 eV, while the adiabatic IP is 8.24 eV. We also observe that the methyl from the *t*-butyl group is not weakened as much as happens in the case of the monomer.

We have also computed the BDEs for two different C–H bonds located on the methoxy and the *t*-butyl group. The BDE values are: E^{BDE}_{C-H} (*methoxy*) = 4.08 eV and E^{BDE}_{C-H} (*t*-butyl) = 4.35 eV, which demonstrate that the proton transfer will be initiated, most likely, from the methoxy group.

4.2.2. MTBE-water mixed clusters

In this section, we present different size $(MTBE)_m$–$(H_2O)_n$ cases completed with a detailed study of their ionized geometries. As a first step, the geometry of the neutral MTBE–water system (see Figure 4a) was obtained using the same level of theory presented above. The intermolecular interaction energy between the MTBE and the water molecule is −7.25 kcal/mol. As regards to the ionization potentials for the MTBE–water complex, the vertical IP is 9.91 eV, while the adiabatic IP is 9.11 eV.

In the case of the $MTBE_2$–water complex, the neutral form is stabilized by two H-bonds between the water molecule and the two MTBE monomers (see Figure 4c). The intermolecular interaction energy is −13.81 kcal/mol, which is mostly given by the H-bond energies between the water and the MTBE monomers. For the ionized $MTBE_2$–water complex we observed that initially the ionization effect takes place on one of the MTBE monomers. The vertical IP energy is 9.66 eV. At end of the geometry optimization, the $MTBE_2$–water complex has changed significantly from its initial geometric configuration. An H^+ has moved from the methyl of the methoxy group of the one MTBE monomer to the oxygen atom of the other MTBE monomer (see Figure 4d). The two MTBE configurations in the dimer–water complex are similar to those obtained in the case of the MTBE dimer, i.e., MTBE–H^+ and $(CH_3)_3$–C–O–CH_2. The adiabatic IP is 8.33 eV, while the intermolecular interaction energy is −30.86 kcal/mol. The NPA analysis gives a more nuanced picture; a 0.55*e* electron charge is located on the H^+, and the total charge of the $(CH_3)_3$–C–O–CH_2 is +0.12*e*, while the total charge of MTBE–H^+ is +0.87*e*. Similar to the MTBE dimer case, we observe significant geometric changes in the C_1–O and O–C_2 bond lengths. In the case of MTBE–H^+, the C_1–O bond lengthens with 0.041 Å, while the O–C_2 bond with 0.075 Å. For the $(CH_3)_3$–C–O–CH_2 subsystem, the C_1–O bond compresses with 0.079 Å, while the O–C_2 lengthens with 0.028 Å, respectively.

For the $(MTBE)_3(H_2O)_2$ ionized mixed cluster, initially the same H^+ proton transfer was observed between two MTBE monomers (Figure 5a) but as a second step, these H^+ has been further transferred from the MTBE–H^+ subsystem to one of the water molecules (Figure 5b), resulting in an H_3O^+ ion (see Figure 5c).

This two-step proton transfer could explain the formation of the stable hydrogen-bound ion clusters that have been demonstrated experimentally in Ref. [12,13] and by us. In the case of ether and ketone-type structures, a combination of $n = m - 2$ for the $X_m(H_2O)_nH^+$ clusters is observed, where X means an ether and ketone-class molecule [12–14].

To study the stability of such ionized clusters, we have performed geometry optimizations on the series of clusters for which m ranges from 2 to 4. Accordingly, for the $m = 2$ ($n = 0$), we obtain the $MTBE_2H^+$, for $m = 3$ ($n = 1$) the $MTBE_3H_2OH^+$ and in the case of $m = 4$ ($n = 2$) the $MTBE_4(H_2O)_2H^+$ complexes. The equilibrium geometries of them are presented in Figure 6a–c, and the C_1–O, C_2–O and H-bond distances are presented in Table 2. Comparing the C_1–O and C_2–O distances, we observe that, for the $m = 2$ case, the distances show the largest values, and, as the size of the mixed cluster grows, the distances become shorter. We observe an approximate 0.02 Å decrease (the difference between $m = 2$ and $m = 4$) for the C_1–O bond, and an approximate 0.03 Å decrease for the C_2–O bond (see Table 2). If we also include the MTBE–H^+ case, one can see that the bond stabilization is more obvious. With regard to the H-bond formed between the water and the MTBE molecules, the bond magnitude increases with the cluster sizes, although is still shorter than the conventional H-bond distance which can be found, for example, between two neutral water

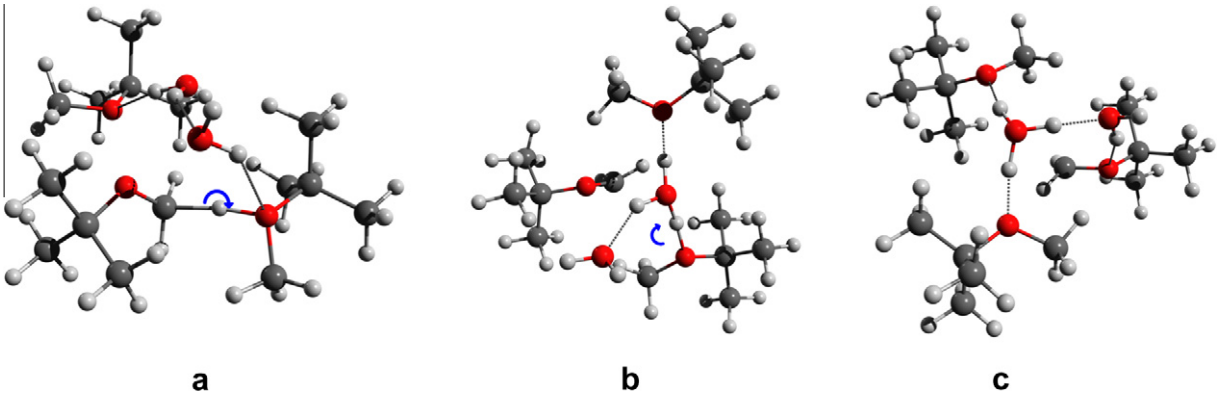

Figure 5. The proton transfer inside the MTBE trimer–water dimer complex. Blue arrows indicate the proton transfer steps. (For interpretation of the references to color in this figure legend, the reader is referred to the web version of this article.)

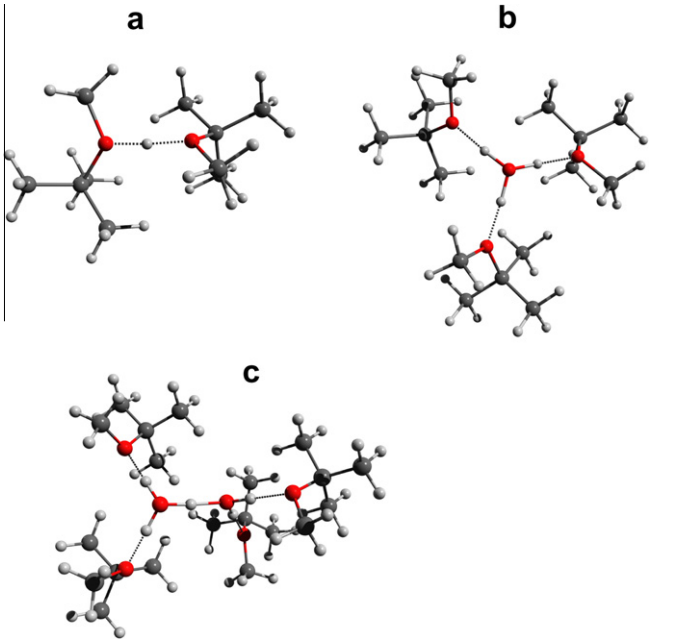

Figure 6. The equilibrium geometric structures of the hydrogen-bonded ion clusters $MTBE_2H^+$ (a), $MTBE_3H_2OH^+$ (b) and $MTBE_4(H_2O)_2H^+$ (c).

Table 2
The C_1–O and C_2–O bond distances (in Å) for the $X_m(H_2O)_nH^+$ hydrogen-bonded ion clusters series with $n = m - 2$.

Structure	C_1–O	C_2–O	H-bond
MTBE	1.405	1.429	–
MTBE–H^+	1.452	1.529	–
$MTBE_2H^+$	1.432	1.477	–
	1.437	1.488	–
$MTBE_3H_2OH^+$	1.421	1.457	1.463
	1.421	1.455	1.461
	1.422	1.454	1.474
$MTBE_4(H_2O)_2H^+$	1.417	1.449	1.633
	1.415	1.448	1.674
	1.422	1.454	1.509
	1.422	1.454	1.524

molecules. The H-bond distance between two water molecules is approximately 1.9 Å, which means that the classical donor–acceptor coupling is loaded with an extra charge transfer effect caused by the ion state. We can conclude that as the cluster size increases, the MTBE geometries get closer to the monomer geometry parameters, which can be explained with the fact that the central water cluster ion removes less and less electron charge from the outer MTBE molecules. If one analyzes the stability of these hydrogen-bonded ion clusters, one can see that, for small values of m, we have stretched C_1–O and C_2–O bonds inside the MTBE. This indicates a significant monomer deformation which is compensated for by the stronger intermolecular interaction between the ion and the MTBE molecule based on strong electrostatic effects. As the cluster size increases, the energy balance shifts toward to the intramolecular direction by having stronger C_1–O and C_2–O bonds inside the MTBE and weaker intermolecular interactions between the ion (H^+, H_3O^+ or $H_5O_2^+$) and the MTBE molecules.

5. Discussion

As widely noted, the ions detected in the photoionization of hydrogen-bonded clusters do not result from the ionization of neutral clusters of the same composition. Instead, inside the neutral cluster, one monomer must fragment to transfer the proton to the ion cluster. This reaction, together with the stability of the resulting ion, dominates the process and affects the mass distribution [25]. We detect mainly protonated clusters, with the only exception being the MTBE dimer. This result led us to suppose that the MTBE ionized dimer is a quite stable ion. The PIE onset of the MTBE dimer is at 9.1 ± 0.1 eV, which is in agreement with the DFT calculations for the ionization potential of MTBE dimer. Interestingly, from the DFT calculation, after the ionization, a proton moves inside the dimer from the methyl of one monomer to the oxygen of the other monomer. This transfer results an ionized dimer with a quite strong electrostatic interaction between the $(CH_3)_3$–C–O–CH_2 parts of a MTBE monomer, with the proton localized mainly on the other MTBE monomer. This electrostatic interaction prevents the dimer from dissociating. Instead, the change in the C_2–O bond distance may lead, to some extent, to a fragmentation of the dimer with the loss of a *t*-butyl group. Thus, the dimer could be the neutral precursor of the fragment detected at $m/z = 119$, even if contributions from heavier clusters cannot be ruled out.

The reaction leading to the detection of protonated MTBE clusters starts from unstable ions and may be represented by the following schemes:

$$((CH_3)_3COCH_3)_m^{\cdot+} \rightarrow ((CH_3)_3COCH_3)_nH^+ + (m-n-1) \times (CH_3)_3COCH_3 + (CH_3)_3COCH_2^{\cdot} \quad (1)$$

Or

$$\rightarrow ((CH_3)_3COCH_3)_nH^+ + (m-n-1)(CH_3)_3COCH_3 + CH_3CO(CH_3)_2CH_2^{\cdot} \quad (2)$$

The $(CH_3)_3COCH_2^{\cdot}$ radical transforms into a *t*-butyl radical and formaldehyde, while the $CH_3CO(CH_3)_2CH_2^{\cdot}$ radical splits into isobutene and a methoxy radical [31]. It is quite difficult to assess to what extend the reactions happen in the cases we consider. From the calculation in Section 4.1, we see that if the C–H bond of the methoxy group is weaker by approximately 6 kcal/mol than the C–H bond in the *t*-butyl group, then the reaction (1) should be favored.

The optimization of the cluster geometries (Section 4) show that for mixed MTBE–water clusters, the proton transfer in the ionized cluster starts on the MTBE molecules. As water molecules are added in the cluster, the proton transfers to the water molecule and form an H_3O^+ core, which gives stability to the ionized cluster. In agreement with these data, the most intense peaks in the heterogeneous protonated cluster distribution $(MTBE)_m(H_2O)_nH^+$ show a magic number distribution given by $n = m - 2$. These numbers correspond to geometrical configurations of Zündel and Eigen water cations with all of the available hydrogen bonding sites interacting with MTBE molecules.

Finally, from the PIE measurements, the ionization energy of the MTBE monomer and its fragment confirm DFT results as well as the ionization energy of MTBE dimer, here presented for the first time.

Our experimental setup does not allow us to retrieve the correct information about fragmentation of the mixed MTBE–water clusters because the appearance energy values of the resulting fragments cannot be rigorously evaluated. However, results from Table 1 suggest that the PIE curve onset values change from $M_2(H_2O)H^+$ cluster to larger clusters. This result suggests, in agreement with DFT calculations, that the ionization dynamic starts to change at the points where $m + n = 3$.

Acknowledgments

T.M. Di Palma acknowledges A. Borghese for the helpful discussions and G. Perretta and B. Sgammato for the technical support. A.

Bende acknowledges financial support from the Romanian National Authority for Scientific Research through the CNCSIS Contracts PCCE-ID 76 and PN-II-ID-PCCE-2011-2-0027. The theoretical calculations have been carried out using the facility at the DataCenter of INCDTIM Cluj-Napoca, for which we gratefully acknowledge their support.

References

[1] G.A. Westphal, J. Cral, T. Brüning, E. Hallier, J. Bünger, Toxicology 268 (2010) 198.
[2] C. Atchen, A. Kolb, W. Putmann, Atmos. Environ. 35 (2001) 6337.
[3] K. Kawamoto, J.S. Arey, P.M. Gschwend, J. Air Waste Manag. Assoc. 53 (2003) 1426.
[4] M.A. Mehalman, Ann. N. Y. Acad. Sci. 982 (2002) 149.
[5] S. Phillips, R.B. Palmer, A. Brody, J. Med. Toxicol. 4 (2008) 115.
[6] T. Garoma, M.D. Gurol, O. Osibodu, L. Thotakura, Chemosphere 73 (5) (2008) 825.
[7] Z. Li, S. Singh, J. Phys. Chem. A 112 (2008) 8593.
[8] F. Gaie-Levrel, C. Gutlé, H.-W. Jochims, E. Rühl, M. Schwell, J. Phys. Chem. A 112 (23) (2008) 825.
[9] A.J. Stace, C. Moore, J. Phys. Chem. 86 (1982) 3681.
[10] S. Wei, W.B. Tzeng Jr., A.W. Castelman, J. Phys. Chem. 95 (1991) 5080.
[11] H.C. Chang, J.C. Jiang, I. Hahndorf, S.H. Lin, Y.T. Lee, H.C. Chang, J. Am. Chem. Soc. 121 (1999) 4443.
[12] T.M. Di Palma, A. Borghese, Nucl. Instrum. Methods Phys. Res., Sect. B 254 (2) (2007) 193.
[13] A. Borghese, T.M. Di Palma, Appl. Opt. 27 (22) (2007) 4948.
[14] T.M. Di Palma, M.V. Prati, A. Borghese, J. Am. Soc. Mass Spectrom. 20 (12) (2009) 2192.
[15] T.M. Di Palma, A. Bende, A. Borghese, Chem. Phys. Lett. 495 (2010) 17.
[16] Y. Zhao, D.G. Truhlar, Theor. Chem. Acc. 120 (2008) 215.
[17] F. Weigend, R. Ahlrichs, Phys. Chem. Chem. Phys. 7 (2005) 3297.
[18] D. Rappoport, F. Furche, J. Chem. Phys. 133 (2010) 134105.
[19] NWChem 6.0 M. Valiev et al., Comput. Phys. Commun. 181 (2010) 1477.
[20] K.L. Schuchardt et al., J. Chem. Inf. Model. 47 (2007) 1045.
[21] J.P. Foster, F. Weinhold, J. Am. Chem. Soc. 102 (1980) 7211.
[22] A.E. Reed, R.B. Weinstock, F. Weinhold, J. Chem. Phys. 83 (1985) 735.
[23] E.D. Glendening, J.K. Badenhoop, A.E. Reed, J.E. Carpenter, J.A. Bohmann, C.M. Morales, F. Weinhold, NBO 5.0, Theoretical Chemistry Institute, University of Wisconsin, Madison, 2001.
[24] A.R. Allouche, J. Comput. Chem. 32 (2011) 174.
[25] B. Brutschy, P. Bisling, E.H. Baumgärtel, Z. Phys. D: At., Mol. Clusters 5 (1987) 217.
[26] O. Kostko, L. Belau, K.R. Wilson, M. Ahmed, J. Phys. Chem. A 112 (2008) 955.
[27] J.H. Gross, Mass Spectrometry –a Textbook, Springer, 2004.
[28] T. Baer, Int. J. Mass Spectrom. 200 (2000) 443.
[29] S.D. Chambreau, J. Zhang, J.C. Traeger, T.H. Morton, Int. J. Mass Spectrom. 199 (2000) 17.
[30] M. Xie, Z. Zhou, Z. Wang, D. Chen, F. Qi, Int. J. Mass Spectrom. 293 (2010) 28.
[31] J.C. Brocard, F. Baronnet, H.E. O'Neal, Combust. Flame 52 (1983) 25.